analytical chemistry

Article

Cite This: *Anal. Chem.* 2019, 91, 4186−4194

pubs.acs.org/ac

Cytometry of Reaction Rate Constant: Measuring Reaction Rate Constant in Individual Cells To Facilitate Robust and Accurate Analysis of Cell-Population Heterogeneity

Vasilij Koshkin,[†] Sven Kochmann,[†] Apinaya Sorupanathan,[†] Chun Peng,[‡] Laurie E. Ailles,[§] Geoffrey Liu,[∥] and Sergey N. Krylov*[,†]

[†]Department of Chemistry and Centre for Research on Biomolecular Interactions, and [‡]Department of Biology and Centre for Research on Biomolecular Interactions, York University, Toronto, Ontario M3J 1P3, Canada

[§]Department of Medical Biophysics, University of Toronto, Toronto, Ontario N5G 1L7, Canada

[∥]Department of Medicine, Medical Oncology, Princess Margaret Cancer Centre, Toronto, Ontario M5G 2M9, Canada

Supporting Information

ABSTRACT: Robust and accurate analysis of cell-population heterogeneity is challenging but required in many areas of biology and medicine. In particular, it is pivotal to the development of reliable cancer biomarkers. Here, we prove that cytometry of reaction rate constant (CRRC) can facilitate such analysis when the kinetic mechanism of a reaction associated with the heterogeneity is known. In CRRC, the cells are loaded with a reaction substrate, and its conversion into a product is followed by time-lapse fluorescence microscopy at the single-cell level. A reaction rate constant is determined for every cell, and a kinetic histogram "number of cells versus the rate constant" is used to determine quantitative parameters of reaction-based cell-population heterogeneity. Such parameters include, for example, the number and sizes of subpopulations. In this work, we applied CRRC to a reaction of substrate extrusion from cells by ATP-binding cassette (ABC) transporters. This reaction is viewed as a potential basis for predictive biomarkers of chemoresistance in cancer. CRRC proved to be robust (insensitive to variations in experimental settings) and accurate for finding quantitative parameters of cell-population heterogeneity. In contrast, a typical nonkinetic analysis, performed on the same data sets, proved to be both nonrobust and inaccurate. Our results suggest that CRRC can potentially facilitate the development of reliable cancer biomarkers on the basis of quantitative parameters of cell-population heterogeneity. A plausible implementation scenario of CRRC-based development, validation, and clinical use of a predictor of ovarian cancer chemoresistance to its frontline therapy is presented.

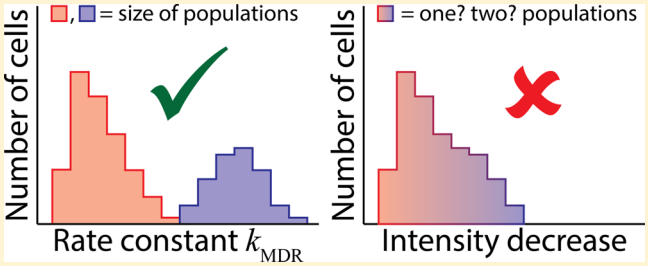

Cell populations within the same tissue are inherently heterogeneous, and this heterogeneity may be so extensive that distinct subpopulations become identifiable.[1,2] For example, populations of cancer cells are comprised typically of at least two subpopulations: bulk tumor cells (that are often sensitive to chemotherapy) and tumor-initiating cells (that are often chemotherapy-resistant).[3,4] In general, cell-population heterogeneity is caused by differences in molecular reactions between the cells. When a specific reaction is associated with cell-population heterogeneity, it can serve as a basis for characterizing this heterogeneity.[5] Measurements of reaction rate constant were used to characterize heterogeneity with a general approach, which we refer to as cytometry of reaction rate constant (CRRC), that results in a kinetic histogram "number of cells versus rate constant".[6−11] CRRC covers all methods that characterize cell population heterogeneity by (i) utilizing the rate constant(s) of a confirmed reaction mechanism and (ii) analyzing a statistically significant number of cells for high-confidence determination of quantitative parameters of cell-population heterogeneity. The kinetic nature of CRRC suggests that it should be able to support robust and accurate characterization of reaction-based cell-population heterogeneity. Accordingly, it may be potentially suitable for the development of reliable cancer biomarkers built upon such heterogeneity.

The concept of CRRC is schematically depicted in Figure 1. First, the cells are loaded with a fluorescent (or fluorogenic) substrate, and the substrate is naturally involved into the cellular reaction of interest. Second, kinetics of change of intracellular substrate concentration is followed by imaging a large number of cells microscopically and measuring the fluorescence intensity in individual cells as a function of time. Third, the reaction rate constant for a known kinetic mechanism of the reaction is determined for every cell.

Received: January 22, 2019
Accepted: February 19, 2019
Published: March 4, 2019

DOI: 10.1021/acs.analchem.9b00388
Anal. Chem. 2019, 91, 4186−4194

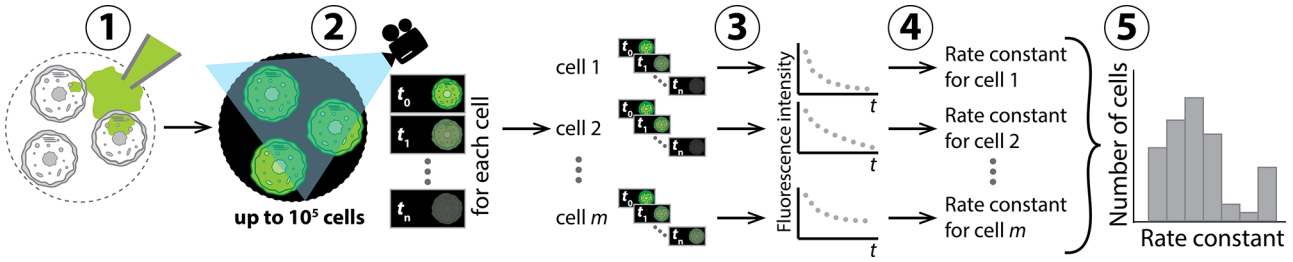

Figure 1. Schematic depiction of cytometry of reaction rate constant. See text for details.

Fourth, the rate constant values are used to construct a kinetic histogram: "number of cells versus the rate constant". The kinetic histogram can be utilized for multifaceted characterization of cell population heterogeneity.

There are a number of quantitative parameters used to characterize cell-population heterogeneity (Figure 2).[12,13] If

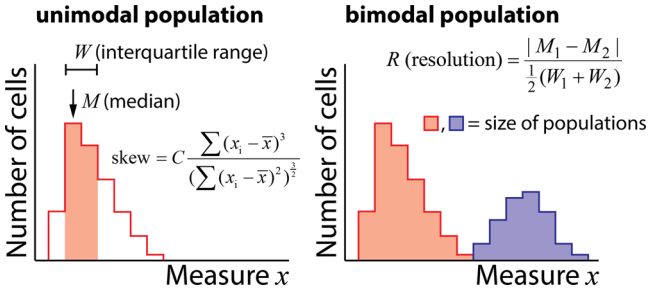

Figure 2. Schematic depiction of unimodal (left) and bimodal (right) cytometry histograms defining quantitative parameters used to characterize cell-population heterogeneity. See text for details.

the cell population is unimodal, it is represented by a single peak in a cytometry histogram "number of cells versus measure x characterizing cells". In classical flow cytometry, x is simply fluorescence intensity. A single peak is comprehensively characterized by peak position (e.g., a median value of x), peak width (e.g., interquartile range), and peak asymmetry (e.g., skewness) (Figure 2, left).[14,15] If the cell population is bimodal, for example, consists of two distinct subpopulations, it is represented by two peaks. For the two subpopulations to be distinguishable, the two peaks should be separated; the quality of separation is characterized by peak resolution (Figure 2, right). The key parameters characterizing a bimodal cell population are sizes of the two subpopulations, which can be found as areas of the corresponding peaks.

In this work, we examined CRRC in its ability to determine the five quantitative parameters characterizing unimodal and bimodal cell populations. The bimodal cell population was created by the controlled mixing of two very closely related cell lines. To place CRRC results in the quantitative context of a non-CRRC approach typically used in such studies, we utilized a typical nonkinetic measure x obtained from the CRRC data sets.

We found that CRRC was robust to variations in experimental conditions, while its nonkinetic counterpart was nonrobust. A 2-fold change in the substrate concentration or analysis time resulted in only less than 16% changes in all heterogeneity parameters determined by CRRC, but in more than 14% and as high as multifold changes of these parameters determined with the nonkinetic analysis. The only exception was the peak width, which was found to be robust in both kinetic and nonkinetic analyses. Importantly, CRRC could determine the size of a small subpopulation in the bimodal cell population with accuracy of approximately 10%, which is likely controlled by the accuracy of preparing the bimodal population via mixing the two cell lines. The robustness and accuracy of CRRC suggest that this approach can potentially facilitate the development of reliable cancer biomarkers based on quantitative parameters of cell-population heterogeneity.

RESULTS

Reaction Choice for CRRC. Substrate extrusion from cells by membrane proteins, known as ATP-binding cassette transporters (ABC transporters), was chosen as a reaction for assessing robustness and accuracy of CRRC.[16] This reaction is a driving force of multidrug resistance (MDR) of cancer cells and is usually called MDR transport.[17] MDR transport should not be confused with MDR: MDR is a clinically observed nonsensitivity of cancer to multiple drugs, while MDR transport is a specific reaction of substrate efflux by ABC transporters. ABC transporters have low substrate specificity, and, therefore, fluorophores can be used as substrates in studies of MDR transport.[18] To avoid misunderstandings, it should be explicitly stated that studying MDR transport does not require fluorescent anticancer drugs.[19]

Nonkinetic histograms were used to characterize MDR-based heterogeneity of cancer cell populations; the size of a cell subpopulation with increased MDR transport activity was used as a heterogeneity parameter to develop predictive biomarkers of clinical resistance of cancer to chemotherapy.[20,21] All such biomarkers, however, have proven to be unreliable clinically,[22,23] likely due to the nonrobustness and inaccuracy of the nonkinetic analysis employed for their derivation. Hence, finding a robust and accurate approach for characterizing MDR-based cell-population heterogeneity may have significant clinical benefits. While the medical relevance of MDR transport served as an important justification for using this reaction in previous studies,[8−11] its use here is mainly a matter of convenience. This work did not aim to prove the suitability of MDR-transport assessment for the development of cancer biomarkers.

Kinetic Mechanism of MDR Transport. Mechanistically, an ABC transporter (T) binds the substrate (S) on the inner side of the membrane, "turns" around, and releases S on the outer side of the membrane (Figure S1).[24] The MDR transport proceeds through the formation of an intermediate complex (TS) and, thus, can be described by the Michaelis−Menten equation (commonly used for enzymatic reactions):[25]

$$\mathrm{T} + \mathrm{S_{in}} \underset{k_{-1}}{\overset{k_1}{\rightleftarrows}} \mathrm{TS} \xrightarrow{k_2} \mathrm{T} + \mathrm{S_{ex}} \qquad (1)$$

DOI: 10.1021/acs.analchem.9b00388
Anal. Chem. 2019, 91, 4186−4194

where S_{in} is intracellular substrate and S_{ex} is extracellular substrate. This process can be characterized by a unimolecular rate constant of MDR transport, k_{MDR}, which is a ratio between the maximum reaction rate, V_{max}, and the Michaelis constant, K_M:[26,27]

$$k_{MDR} = V_{max}/K_M \quad (2)$$

Our earlier work has proven that the single-cell kinetics of MDR follow the Michaelis–Menten mechanism,[8−11] and, thus, k_{MDR} (as defined above) is suitable for the analysis of MDR-based cell-population heterogeneity by CRRC.

Timeline of a CRRC Experiment for MDR Transport. The timeline of our experiment is schematically shown in Figure 3 (for a single cell). The experiment starts with cells

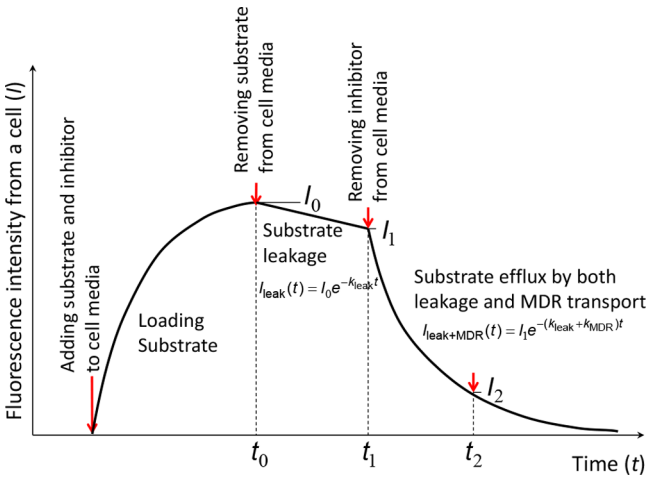

Figure 3. Schematic depiction of the timeline of CRRC experiment aiming to determine the rate constant of MDR efflux, k_{MDR}. See text for details.

being in a Petri dish on a microscope stage. A fluorescent substrate of MDR transport and an inhibitor of ABC transporters are added simultaneously to the cell media to initiate substrate loading into the cells. When fluorescence intensity from a cell approaches its saturation at level I_0, the substrate loading is stopped by removing the extracellular substrate while keeping the inhibitor in the media. This initiates the "substrate leakage" process that includes both passive substrate diffusion from the cell and photobleaching of the intracellular substrate. The substrate leakage process is accompanied by fluorescence intensity decrease to level I_1. The MDR-mediated efflux then is initiated by removing the MDR-transport inhibitor, and the cumulative substrate loss by both the substrate leakage process and the MDR transport is followed.

A kinetic curve of substrate efflux consists of (i) an initial segment (from t_0 to t_1) representing the substrate leakage process and (ii) the main segment (after t_1) that corresponds to the cumulative effect of the substrate leakage process and MDR transport. The substrate leakage process from a cell is accompanied by exponential decrease of cellular fluorescence intensity:

$$I_{leak}(t) = I_0\, e^{-k_{leak}t} \quad (3)$$

where I_0 is the initial intensity, and k_{leak} is a unimolecular rate constant characterizing the substrate leakage process. Fluorescence intensity decreases to I_1 relatively slowly so that $(I_0 - I_1)/I_0 \ll 1$. This allows the calculation of k_{leak} from the near linear initial segment using the following approximate equation:

$$k_{leak} \approx \frac{I_0 - I_1}{I_0}\frac{1}{(t_1 - t_0)} \quad (4)$$

This value of k_{leak} can then be used to determine k_{MDR} from the main exponential segment of the kinetic trace.

The decrease of fluorescence intensity caused by MDR transport after t_1 is also exponential (provided that $[S_{in}] \ll K_M$):

$$I_{MDR}(t) = I_1\, e^{-k_{MDR}t} \quad (5)$$

The cumulative substrate efflux is driven by two first-order processes (leakage and MDR transport) and is, therefore, also the first-order process. It is accompanied by an exponential decrease of cellular fluorescence intensity with a cumulative rate constant $k_{leak} + k_{MDR}$:

$$I_{leak+MDR}(t) = I_1\, e^{-(k_{leak}+k_{MDR})t} \quad (6)$$

Note that I_0, k_{leak}, I_1, and k_{MDR} are unique for every cell. The value of k_{MDR} for a single cell is determined from a single kinetic curve by finding k_{leak} from eq 4 and placing it in eq 6, which is then used to fit the main segment on this kinetic curve with k_{MDR} being a variable parameter. If $k_{leak} \ll k_{MDR}$, the procedure of k_{MDR} determination can be simplified by neglecting k_{leak} and finding k_{MDR} from the main segment on the kinetic trace (after t_1) using eq 5.

Robustness and accuracy of our kinetic analysis were studied in comparison to those of the common nonkinetic analysis of the same data set. A kinetic curve utilized for finding k_{MDR} (see Figure 3) was also used to calculate a nonkinetic measure of MDR transport, a relative decrease of fluorescence intensity, $(I_1 - I_2)/I_1$,[28−30] and construct the nonkinetic histogram "number of cells versus $(I_1 - I_2)/I_1$". The value of $(I_1 - I_2)/I_1$ corresponds to a fraction of the MDR substrate extruded from the cell.

Experimental Design for Assessing Accuracy and Robustness of CRRC. In this study, we used two types of A2780 cultured ovarian cancer cells: a drug-sensitive parental cell line with a basal MDR activity and its derivative drug-resistant subline with increased MDR activity.[31] The drug-sensitive line models bulk tumor cells, while the drug-resistant subline models tumor-initiating cells.[32] Fluorescein was used as a substrate of MDR transport (a known substrate for the MRP-type ABC transporters predominantly expressed in these cells),[33] and glyburide was used as an inhibitor of MRP transporters.[34]

The choice of substrate concentration is governed, in general, by two considerations. On one hand, the substrate concentration should be as high as possible to facilitate a maximum dynamic range of fluorescent measurements. On the other hand, the value of substrate concentration should be much less that the value of K_M to ensure the first-order regime of substrate efflux required for applicability of eq 6. A rule of thumb is to choose the substrate concentration that is 1 order of magnitude below K_M. In our case, the literature data suggest K_M as low as 14 μM for fluorescein in the reaction depicted in eq 1.[33,35] Thus, fluorescein concentration should not exceed 3.0 μM. Any experimental protocol should be robust to changes in substrate concentration within a meaningful range, for example, within $\sqrt{2}$-fold in either direction from the

DOI: 10.1021/acs.analchem.9b00388
Anal. Chem. 2019, 91, 4186−4194

concentration of choice.[36] If we choose fluorescein concentration of 2.12 μM as a "protocol concentration", then the range will be from 1.5 to 3.0 μM. An additional advantage of ensuring the first-order regime is that it renders the assay calibration-free (intracellular substrate concentration does not need to be known) and, thus, increases its reliability and robustness.

Time-lapse fluorescence imaging of all cells in the field of view with 3 min intervals started after replacing fluorescein-containing media with fluorescein-free media (t_0 in Figure 3) and ended after 2−3 h. The images are archived in supporting file Timeseries.zip. Individual cells were identified in every image and traced through the entire time series. Mean fluorescence intensity for every cell in a single image was calculated and used to create a kinetic curve for every cell (Note S1). We found that for our experimental system $k_{leak} < 0.1 \times k_{MDR}$, and, therefore, eq 5 was used instead of eq 6 for finding k_{MDR}. The values of k_{MDR} and $(I_1 - I_2)/I_1$ were determined as described above and used to construct kinetic and nonkinetic histograms, respectively (archived in supporting file Plotteddata.zip). The above-described procedures were used for three sets of experiments that assessed the quantitative performance of the kinetic analysis as well as of the nonkinetic one.

Analysis of Heterogeneity of a Unimodal Histogram. In the first set of experiments, we compared the robustness of the kinetic and nonkinetic analyses in characterizing heterogeneity of a unimodal histogram (containing only a single peak) obtained for the drug-sensitive cell line. Substrate concentration and observation time are typical variable parameters.[37] Even when protocols prescribe a specific concentration and a specific observation time, these parameters vary from experiment to experiment due to inaccuracy of measuring devices, human errors, attempts to optimize protocols (e.g., via shortening observation time), etc. Such variations may cause nonrobustness of the analysis. Such nonrobustness is further aggravated when different laboratories use protocols and integrate them into other practices, such as surgical protocols, etc. Therefore, we studied the robustness of analysis results to variations in fluorescein concentration and observation time. The parental drug-sensitive cell line was used in this part of our study.

To understand analysis robustness to substrate concentration, we utilized two fluorescein concentrations in the cell media, 1.5 and 3.0 μM; the justification for this choice was provided above. An observation time of 2 h is common for MDR assays;[38,39] it was used as a default value throughout this study. Note that longer substrate-loading times will be required if spheroids or tissue slices are used instead of dispersed cells. Also, CRRC studies of slower transport or enzymatic processes will require longer time-lapse observations to unsure the conversion of most of the substrate into the product. Fluorescence images of >1000 cells each were processed (kinetic traces for all cells are archived in Kinetictraces.zip), and kinetic and nonkinetic histograms were plotted (Figure 4, top). As expected for a pure cell line, both histograms were unimodal and could be characterized by the median values of k_{MDR} and $(I_1 - I_2)/I_1$, respectively, interquartile range (a measure of peak width), and peak skewness (a measure of peak asymmetry).[15]

Doubling the substrate concentration did not cause significant changes in the kinetic histogram (Figure 4, top, left): the median value of k_{MDR}, the interquartile range, and

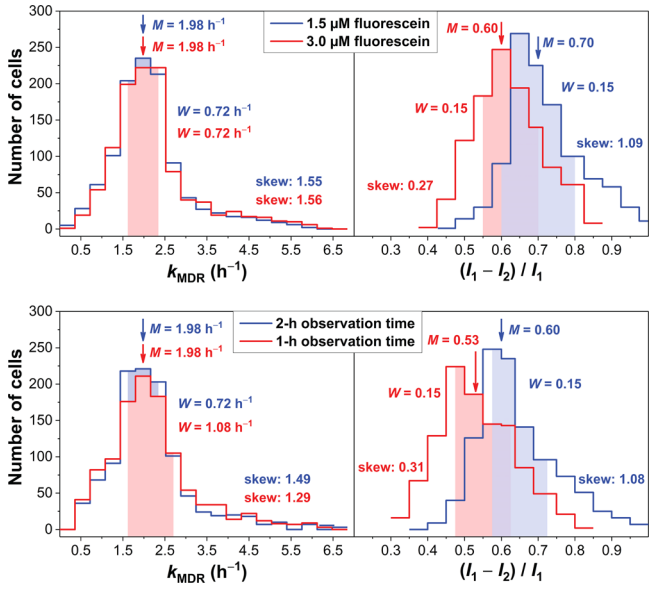

Figure 4. Effect of 2-fold changes in substrate concentration (top) and observation time (bottom) on kinetic (left) and nonkinetic (right) histograms obtained from single-cell time dependence of intracellular fluorescence of MDR substrate. The arrows indicate positions of median k_{MDR} and $(I_1 - I_2)/I_1$ for the respective peaks.

peak skewness changed not more than 3% (k_{MDR}, both 1.98 h^{-1}; interquartile range, 0.72 and 0.72 h^{-1}, and skewness, 1.55 and 1.56). In contrast, the nonkinetic analysis (Figure 4, top, right) revealed a much greater dependence of these parameters on the substrate concentration. Upon increasing fluorescein concentration from 1.5 to 3.0 μM, the median value of $(I_1 - I_2)/I_1$ decreased from 0.70 to 0.60 ($p < 0.05$ for the entire experimental set), and skewness dropped from 1.09 to 0.27 ($p < 0.01$ for the entire experimental set). Thus, the kinetic analysis was very robust to changing substrate concentration while its nonkinetic counterpart showed rather dramatic nonrobustness.

We then studied the robustness of the kinetic and nonkinetic analyses with regards to shortening the observation time in the assay. In general, shortening the observation time is beneficial as it allows for a faster assay. Accordingly, the values of k_{MDR} and $(I_1 - I_2)/I_1$ were determined from the default 2-h kinetic traces and from truncated 1-h traces for each of >1000 cells (archived in Kinetictraces.zip), and kinetic and nonkinetic histograms were constructed for 2- and 1-h observation times (Figure 4, bottom). The results were similar to those for the different substrate concentrations. The effects of changing observation time on the median value of the MDR transport measure and peak skewness were much greater for the nonkinetic analysis (Figure 4, bottom, right) than for the kinetic analysis (Figure 4, bottom, left).

To summarize, the results of experiments with different substrate concentrations and different observation times proved that the kinetic CRRC analysis, in contrast to its nonkinetic counterpart, was robust to variations in two major assay conditions, when used to determine parameters of a unimodal distribution in the histogram.

Resolving Drug-Sensitive and Drug-Resistant Cells. In the second set of experiments, we assessed the ability of the kinetic and nonkinetic analyses to distinguish cells with different levels of MDR activity, to resolve the drug-sensitive cell line from the drug-resistant subline. The concentration of

DOI: 10.1021/acs.analchem.9b00388
Anal. Chem. 2019, 91, 4186−4194

substrate was 1.5 μM, and the observation time was 2 h. Single-cell kinetic traces were recorded for the drug-sensitive line and drug-resistant subline (>1000 cells each), in two separate experiments (archived in Kinetictraces.zip). The values of k_{MDR} and $(I_1 - I_2)/I_1$ were found as described above and used to construct kinetic and nonkinetic histograms, respectively, for both types of cells (Figure 5).

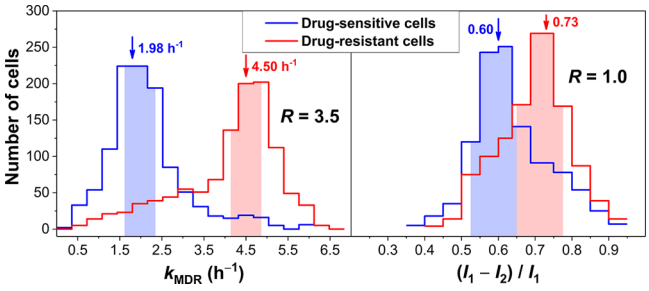

Figure 5. Resolution of peaks corresponding to the drug-sensitive cell line (with basal MDR activity) and drug-resistant subline (with elevated MDR activity) in kinetic (left) and nonkinetic (right) histograms obtained from single-cell time dependence of intracellular fluorescence of MDR substrate. The vertical arrows indicate positions of median values of k_{MDR} and $(I_1 - I_2)/I_1$, and the shaded areas show interquartile ranges for the respective peaks.

The median values of k_{MDR} for the resistant and sensitive cells differed by a factor of 2.3. The median value of $(I_1 - I_2)/I_1$ for resistant and sensitive cells differed only by a factor of 1.2. Resolution R of peaks corresponding to drug-resistant and drug-sensitive cells was defined as

$$R = \frac{|M_1 - M_2|}{\frac{1}{2}(W_1 + W_2)} \quad (7)$$

where M_1 and M_2 are the median values of the two distributions (drug-sensitive and drug-resistant), and W_1 and W_2 are their widths calculated as interquartile ranges.[15] On the basis of the histograms in Figure 5, resolution between the peaks in the kinetic assay was 3.5; in the nonkinetic assay it was only 1.0 ($p < 0.05$ for the entire experimental set). For accurate analysis of the peaks, a resolution of 1.5 (i.e., baseline resolution) is required.[40] These results proved that the kinetic assay had a much greater resolving power than the nonkinetic one for two subpopulations with different reaction rates.

Determining Size of a Subpopulation of Drug-Resistant Cells. In the third and final set of experiments, we assessed the ability of kinetic and nonkinetic analyses to determine robustly and accurately the size of a small subpopulation of cells with a reaction rate distinct from that of a larger subpopulation. A bimodal cell population required for such a study was prepared by mixing 80% of the drug-sensitive cells with 20% of the drug-resistant cells. The accuracy of preparation for the small subpopulation was approximately 10% due to intrinsic heterogeneity of each subpopulation and errors in cell counting.

The experiments for the bimodal cell populations were conducted for two different substrate concentrations, 1.5 and 3.0 μM, to test analysis robustness with regards to the varying substrate concentration. Fluorescence images were processed to determine k_{MDR} and $(I_1 - I_2)/I_1$ for each of 791 cells (archived in Kinetictraces.zip), and the corresponding kinetic and nonkinetic histograms were plotted (Figure 6; archived in Plotteddata.zip).

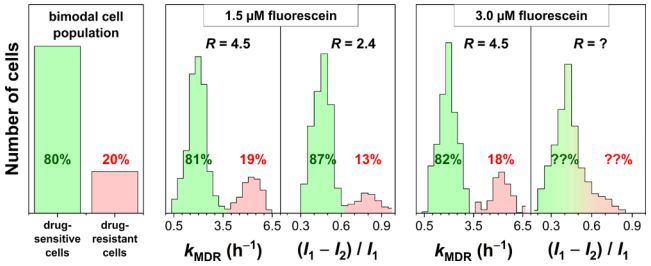

Figure 6. Quantitation of the relative size of drug-resistant cells in a bimodal cell population consisting of both drug-resistant and drug-sensitive cells. The left panel illustrates the composition of the bimodal cell population, which was made by mixing drug-resistant and drug-sensitive cells at a 1:4 ratio. The middle and right panels show the comparison of kinetic and nonkinetic histograms for 1.5 and 3.0 μM fluorescein. Question marks reflect an inability to distinguish between cell populations.

Because the drug-resistant subline had 2.3 times higher k_{MDR}, the kinetic histogram was bimodal for both concentrations of fluorescein. The resolution was 4.5 for both 1.5 and 3.0 μM, respectively, suggesting great robustness of CRRC in peak resolution. The relative area of the peak with higher k_{MDR} is defined by the fraction of drug-resistant cells in the cell population, which was 20% in our experiments. The measured values of this relative area were 19% and 18% for 1.5 and 3.0 μM fluorescein, respectively. A deviation of less than 10% from the expected value proved that the kinetic analysis was both accurate and robust with regards to variations in the substrate concentration.

In contrast, the nonkinetic analysis was nonrobust in resolving the peak. When the concentration of fluorescein increased from 1.5 and 3.0 μM, resolution dropped from 2.4 to uncertain as the second peak disappeared. Obviously, such nonrobustness is detrimental for analytical use of the nonkinetic approach. Further, the nonkinetic analysis was both nonrobust and inaccurate in finding the size of drug-resistant subpopulation. The measured size was 13% for 1.5 μM fluorescein (over 30% difference from the actual size), while the size could not be determined at all for 3.0 μM fluorescein due to the lacking peak resolution. At 3.0 μM fluorescein, the nonkinetic histogram became unimodal with no boundary between the drug-sensitive and drug-resistant peaks. Thus, the kinetic analysis of the size of a subpopulation of cells with a distinct MDR transport rate was both robust and accurate, while the nonkinetic analysis lacked both robustness and accuracy.

Challenges associated with quantifying a relatively small cell subpopulation in the presence of a relatively large one are similar to those arising in quantifying a small peak adjacent to a large one in chromatography. Approaches suitable for addressing these challenges are also similar to the chromatographic ones: the small peak should be resolved from the large peak, and the size of the small peak should be greater than the limit of quantitation. In the context of subpopulation analysis, these requirements translate to the following. In addition to a good resolution of the peaks, a statistically significant number of cells in the small subpopulation are required for its reliable identification and for accurate and robust measurement of its

DOI: 10.1021/acs.analchem.9b00388
Anal. Chem. 2019, 91, 4186−4194

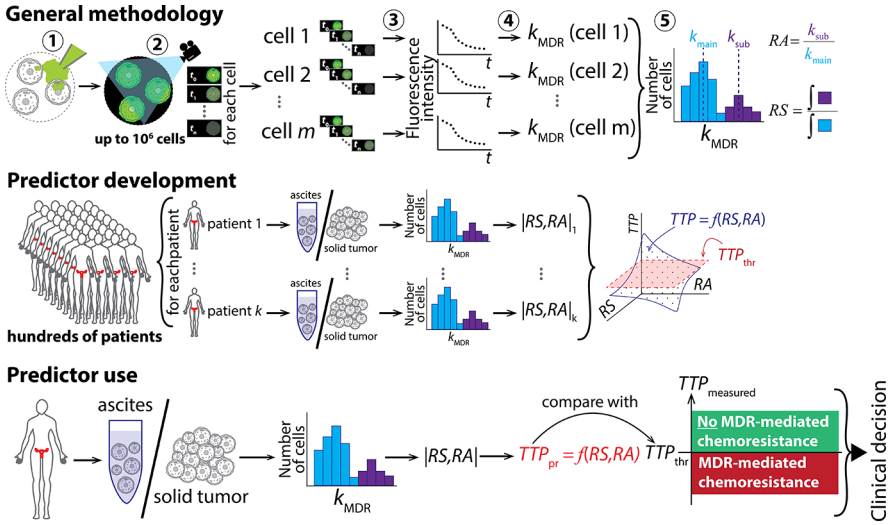

Figure 7. Scenario of using MDRmetry for development, validation, and clinical utilization of a predictor of ovarian cancer resistance to its frontline therapy. See text for detailed explanation.

size. The total number of cells analyzed should increase with decreasing relative size of the small subpopulation.

DISCUSSION

The demonstrated robustness and accuracy of CRRC suggest that it should be preferred over the nonkinetic approach for discovery and validation of disease biomarkers based on cell-population heterogeneity. Discovery and validation of biomarkers require the analysis of a thousand or more clinical samples and processing them as a single data set. This large number of samples necessitates the participation of multiple hospitals and analytical laboratories and the availability of a quantitatively robust protocol. Such a protocol can be supported by CRRC but not by the nonkinetic approach. Indeed, let us hypothetically consider that CRRC is used for the development and validation of biomarkers based on the relative size of the resistant subpopulation determined from the kinetic histogram "number of cells versus k_{MDR}". Let us also assume that an optimum protocol for measuring the relative size of the resistant subpopulation is developed. This protocol will be used by personnel in a large number of laboratories to accumulate a sufficient data set. Let us further assume that the protocol is based on [Substrate] = 2.25 μM. Substrate concentration can vary from analysis to analysis by a factor of $\sqrt{2}$ due to multiple factors including but not limited to inaccuracy of measuring devices and human errors. The CRRC approach can withstand this variation in substrate concentration and recover the accurate size of the resistant subpopulation while the nonkinetic approach becomes absolutely inaccurate. As a result, an attempt to validate a biomarker with the nonkinetic approach will fail due to method nonrobustness. This failure will result in a tremendous loss of human and material resources put into the development and validation effort. In contrast, the accuracy and robustness of CRRC will provide a realistic chance to successfully develop and validate biomarkers based on the relative size of resistant cell subpopulation. Furthermore, CRRC can be potentially applied to tumor types for which tumor initiating cells could not be reliably identified with classical methods.[22]

It is important to emphasize that the development of biomarkers, in particular, those that are based on cell-population heterogeneity, is also hindered by "biological non-robustness and inaccuracy". There may be significant intrinsic sample-to-sample variation in cell-population heterogeneity parameters associated with the biological difference between the samples. For example, we observed a difference in peak resolution between experiments with earlier passages (Figure 5) and later passages (Figure 6) of cells. Such differences obviously cannot be compensated but can be studied with CRRC. Having a robust and accurate cytometric method eliminates doubts in the origin of variations; if any variations are observed, they are biological rather than methodological.

We coin a new term, MDRmetry, for the adaptation of CRRC to assess the MDR-based heterogeneity that is outlined in this study. MDRmetry will be important practically for continuing attempts to develop accurate predictors of MDR-mediated chemoresistance in cancer. When research funds became available, we will use MDRmetry to develop and validate a reliable predictor of chemoresistance of ovarian cancer to its frontline platinum/taxane therapy. Our current study proved that MDRmetry can accurately determine two parameters comprehensively characterizing the drug-resistant subpopulation: its relative size (*RS*, ratio between numbers of cells in the drug-resistant and main drug-sensitive subpopulations) and relative activity (*RA*, ratio between median k_{MDR} values of the drug-resistant and main drug-sensitive subpopulations) (Figure 7, top). Our current study also proved that |*RS*,*RA*| (a combination of *RS* and *RA* for a specific specimen) is robust to changes in the concentration of MDR substrate and observation time. We will, thus, be building a predictor based on accurate and robust measurements of |*RS*,*RA*|.

The predictor will be developed and validated using the following approach (Figure 7, middle). Tumor tissues will be collected from patients before the application of primary chemotherapy. |*RS*,*RA*| will determined for every specimen. Time to tumor progression (*TTP*, a measure of cancer response to therapy) after primary chemotherapy will be accurately determined for every patient. An accurate and robust three-dimensional predictor plot *TTP* versus |*RS*,*RA*| will be constructed on the basis of *TTP* and |*RS*,*RA*| data

DOI: 10.1021/acs.analchem.9b00388
Anal. Chem. 2019, 91, 4186−4194

collected in different facilities to achieve the statistically significant number of patients (the accuracy and robustness of *TTP* and |*RS*,*RA*| allow pooling these data into a single set). Further, a predictor function $TTP = f(RS,RA)$ will be derived by fitting the points in the predictor plot with a polynomial function. The predictor function will be validated with the |*RS*,*RA*,*TTP*| data obtained by using tissues from another pool of patients of a statistically significant size.

If the developed predictor is successfully validated, it will be clinically utilized as follows (Figure 7, bottom). Tumor tissue will be collected from a patient to be tested before applying primary chemotherapy. |*RS*,*RA*| will determined, and the predicted *TTP* (TTP_{pr}) will be calculated from the validated predictor function: $TTP_{pr} = f(RS,RA)$. This value will be compared to the clinically accepted threshold *TTP*: TTP_{thr}. If $TTP_{pr} < TTP_{thr}$, the patient will be deemed to have MDR-dependent chemoresistance, and an alternative treatment will be considered instead of primary chemotherapy. If $TTP_{pr} \geq TTP_{thr}$, then primary chemotherapy should be used, while chances remain that the patient will present with MDR-independent chemoresistance driven by the other two major resistance mechanisms: drug degradation by intracellular enzymatic cascades and repair of drug-induced DNA damage by nuclear enzymes.[41,42] It is important to emphasize that CRRC-based technologies similar to MDRmetry can be created and used for the development of predictors based on activities of the two additional drug-resistance mechanisms. Further, we envision the development of a "cumulative" chemoresistance predictor built upon all three drug-resistance mechanisms. Such predictors belong to a class of activity-based biomarkers; their development requires more analytical insights, but they are viewed as potentially more accurate than expression-based biomarkers.

CRRC has been applied only to cell suspension so far. We foresee that CRRC can potentially be applied to intact live-tissue slices, but such an application is more challenging methodologically. We have conducted some preliminary work with spheroids and found that cells dispersed from spheroids retain their phenotype during 96 h.[43,44] Therefore, our initial plan is not to use intact tissue slices but to use cell suspensions prepared by dispersal of tissue specimens.

CRRC has a few limitations. First, CRRC requires that a kinetic mechanism of the reaction of interest be known; in essence, this requirement necessitates a separate experimental study to confirm this mechanism. Some research on kinetic mechanisms of clinically relevant cellular reactions has already been conducted.[45] We expect that our results will convince equipped laboratories to focus on such kinetic studies. Second, in the presented here version of CRRC, the initial substrate concentration in cells should be in the range needed for the first-order assumption; on the other hand, it should be within the dynamic range of fluorescence detection. This requirement may become very limiting if the substrate concentration that satisfies the first-order assumption is too low for the kinetic traces to be recorded. For example, a Michaelis mechanism with $K_M = 0.1\ \mu M$ requires that the initial intracellular substrate concentration be as low as 10 nM, which is below the limit of quantitation of regular fluorescence microscopes. This limitation may be overcome by abandoning the requirement for first-order kinetics; we have previously demonstrated CRRC-based determination of K_M and V_{max} via non-first-order kinetic analysis followed by finding k_{MDR} with eq 2.[10] It is important to note that using non-first-order kinetics makes the analysis noncalibration-free; for example, finding K_M requires knowing intracellular substrate concentration, which is impossible without calibrating fluorescent signal with respect to substrate concentration. Improving signal-to-noise ratio in fluorescence microscopy is an attractive way of overcoming the limitation of substrate concentration without abandoning the first-order approximation. This study may serve as a motivation for efforts aiming to find technical solutions for such improvements. Some approaches utilized in highly sensitive fluorescence detectors can be potentially transferred to fluorescence microscopy of live cells.[46,47] Third, CRRC becomes much more difficult to implement when more than one reaction constant needs to be determined for the same reaction. Determining more than one constant may require measuring kinetic traces for each cell under different conditions, for example, under different starting substrate concentrations; such measurements may be very cumbersome. It should be noted that the above limitations are a natural cost of the analytical advantages of CRRC, its quantitative accuracy and robustness.

Modern microscopes and image processing software allow automation of CRRC for fast and reliable acquisition of kinetic data for thousands of cells, a requirement for determining statistical significance of the heterogeneity parameters. The availability of required hardware and software suggests that the use of CRRC can gain momentum rapidly. We foresee that CRRC will potentially facilitate the development of reliable disease biomarkers based on parameters of reaction-based cell-population heterogeneity.[48−52] We also envision a multiplexed version of CRRC, in which several parameters (e.g., cell status, phenotypes, kinetic constants of parallel processes) are evaluated either in parallel or sequentially.[8]

MATERIALS AND METHODS

Cell Preparation. Cells were grown and prepared by following standard procedures published elsewhere.[27] Briefly, human ovarian carcinoma cells A2780, and their cisplatin-resistant variant A2780-cp, were grown under standard cell culture conditions in Dulbecco's Modified Eagle's medium (DMEM; supplement liquid containing 4500 mg L^{-1} of glucose, 1500 mg L^{-1} of sodium bicarbonate, 1 mM of sodium pyruvate, and 4 mM of L-glutamine) at 37 °C in a humidified atmosphere of 5% CO_2. DMEM produced by ATCC (30-2002) was purchased from Cedarlane (Burlington, Ontario, Canada). The cell culture medium contained conventional supplements (100 IU mL^{-1} penicillin, 100 μg mL^{-1} streptomycin, and 10% fetal bovine serum) purchased from Invitrogen (Burlington, Ontario, Canada).

Image Acquisition. Single cells were dispersed in 35 mm dishes at 60−80% confluence in cell-support medium (self-prepared Krebs-Ringer bicarbonate buffer, KRB-buffer) containing 115 mM NaCl, 5.9 mM KCl, 2.5 mM $CaCl_2$, 1.2 mM $MgCl_2$, 1.2 mM NaH_2PO_4, 15 mM $NaHCO_3$, 10 mM glucose; pH of KRB-buffer was 7.4. Fluorescein (1.5 μM or 3.0 μM; see main text) and glyburide (10 μM; also called glibenclamide), an MDR transport inhibitor,[34] were added to the cell suspension for substrate and inhibitor loading into the cells. The loading was continued until fluorescence intensity approaches its saturation at level I_0 (Figure 3). Reagents were obtained from Sigma-Aldrich (Oakville, Ontario, Canada), Fluka AG (Buchs, Switzerland), and BDH Chemicals Ltd. (Poole, England).

DOI: 10.1021/acs.analchem.9b00388
Anal. Chem. 2019, 91, 4186−4194

The loading was stopped by removing the extracellular substrate by gently replacing the cell support medium with fresh KRB-buffer supplemented with 10 μM glyburide (inhibitor) but not with fluorescein. This initiated passive substrate leakage through the membrane was accompanied by a fluorescence intensity decrease to level I_1 (Figure 3). Leakage was monitored by a fluorescence microscope (see below). Finally, the MDR-mediated efflux was initiated by replacing the cell support medium with pure KRB-buffer (i.e., no inhibitor, no substrate). The fluorescence intensity decrease (caused by the MDR transport) was further monitored.

Time-lapse fluorescence imaging of all cells in the field of view with 3 min intervals started after replacing fluorescein-containing media with a fluorescein-free one (t_0 in Figure 3) and ended after 2−3 h. Imaging was performed with an Olympus Fluoview FV300 laser scanning confocal fluorescence microscope, using an argon-ion laser (Melles Griot; λ_{exc} = 488 nm; maximum power of 100 mW; used at 10% intensity) and an Omega Optical XF75 filter set. Images were acquired with an open pinhole to collect signal from the whole depth of the cell. Excitation scans were done using a 10× lens; each full picture scan took 1.69 s. For each time series, the dynamic range of imaging had to be adjusted to prevent signal saturation in highly loaded cells; the majority of images were taken with 600−700 V photomultiplier (PMT) voltage, 1.0× gain, and 10% offset.

For each experiment, 3−4 time-series, each covering another 200−400 cells, were recorded as TIF-files, each containing 40−60 images (2−3 h recording in 3 min intervals); TIF-files are archived in Timeseries.zip. We organized the time series to correspond to their respective figures in the main text; color names in brackets of the folder name refer to the respective colors of the curve in the figures.

Extraction and Analysis of Kinetic Traces. The time series were evaluated using ImageJ software with the Time Series Analyzer V3 plugin to obtain kinetic traces for 1092 cells per experiment. Each single-cell trace was transferred to OriginPro software and subjected to kinetic and nonkinetic assessment. There was a small fraction of cells showing a very rapid decrease of fluorescence intensity. Such a fast loss of intracellular substrate was considered to be a sign of cell damage. A viability marker can be in principle included in analysis to assess plasma membrane integrity.[8] However, in the current study, we simply excluded these cells from further analysis; after excluding these cells, each data set still contained over 1000 cells. The kinetic assessment is illustrated using a sample kinetic trace in Figure S2. Briefly, the rate constant of leakage (k_{leak}) was determined from a linear fit of the initial segment, while the cumulative rate constant (k_{total}) of both leakage and MDR efflux ($k_{leak} + k_{MDR}$) was determined simply from an exponential fit of the main segment (see eq 5) because, for the majority of A2780 cells, the contribution of k_{leak} was negligible in our system. For nonkinetic assessment parameter $(I_1 - I_2)/I_1$ was determined for each trace. Further details on the extraction and analysis can be found in Note S2.

Cell Population Analysis. MDR transport of an entire cell population of one experiment was characterized by histograms presenting distributions of individual cell k_{MDR} and $(I_1 - I_2)/I_1$. Histograms were plotted in OriginPro software using Automatic Binning mode, and characterized by median, interquartile range (middle 50%), and skewness coefficient (adjusted Fisher−Pearson standardized moment coefficient[53]). All of these parameters were determined using OriginPro's Descriptive Statistics tool. The final histogram data together with the plots of Figures 4−5 are archived in Plotteddata.zip.

■ ASSOCIATED CONTENT

Supporting Information

The Supporting Information is available free of charge on the ACS Publications website at DOI: 10.1021/acs.analchem.9b00388.

Figure S1, note S1, Extracting kinetic traces from cell images; Note S2, Analysis of kinetic traces, Figure S2 (PDF)

Images of time series (ZIP)

Kinetic traces (ZIP)

Histogram plots (ZIP)

■ AUTHOR INFORMATION

Corresponding Author

*E-mail: skrylov@yorku.ca.

ORCID

Sven Kochmann: 0000-0001-7423-4609

Sergey N. Krylov: 0000-0003-3270-2130

Notes

The authors declare no competing financial interest.

■ ACKNOWLEDGMENTS

This work was supported by the NSERC Discovery grant (no. 238990) to S.N.K.

■ REFERENCES

(1) Huang, S. *Development* **2009**, *136*, 3853−62.

(2) Altschuler, S. J.; Wu, L. F. *Cell* **2010**, *141*, 559−63.

(3) Kwon, M. J.; Shin, Y. K. *Int. J. Mol. Sci.* **2013**, *14*, 6624−48.

(4) McIntosh, K.; Balch, C.; Tiwari, A. K. *Expert Opin. Drug Metab. Toxicol.* **2016**, *12*, 633−44.

(5) Mantzaris, N. V. *Biophys. J.* **2007**, *92*, 4271−88.

(6) Kubitscheck, U.; Pratsch, L.; Passow, H.; Peters, R. *Biophys. J.* **1995**, *69*, 30−41.

(7) Sunray, M.; Zurgil, N.; Shafran, Y.; Deutsch, M. *Cytometry* **2002**, *47*, 8−16.

(8) Koshkin, V.; Krylov, S. N. *Anal. Chem.* **2011**, *83*, 6132−4.

(9) Koshkin, V.; Krylov, S. N. *PLoS One* **2012**, *7*, No. e41368.

(10) Koshkin, V.; Krylov, S. N. *Anal. Chem.* **2013**, *85*, 2578−81.

(11) Koshkin, V.; Yang, B. B.; Krylov, S. N. *PLoS One* **2013**, *8*, No. e79222.

(12) Gough, A.; Stern, A. M.; Maier, J.; Lezon, T.; Shun, T. Y.; Chennubhotla, C.; Schurdak, M. E.; Haney, S. A.; Taylor, D. L. *SLAS Discovery* **2017**, *22*, 213−37.

(13) Delvigne, F.; Baert, J.; Gofflot, S.; Lejeune, A.; Telek, S.; Johanson, T.; Eliasson Lantz, A. E. *J. Chem. Technol. Biotechnol.* **2015**, *90*, 314−23.

(14) Peggs, K. S.; Verfuerth, S.; D'Sa, S.; Yong, K.; Mackinnon, S. *Br. J. Haematol.* **2003**, *120*, 154−65.

(15) Henderson, A. R. *Clin. Chim. Acta* **2006**, *366*, 112−29.

(16) *ABC Transporters and Multidrug Resistance*; Boumendjel, A., Boutonnat, J., Robert, J., Eds.; John Wiley & Sons: Hoboken, NJ, 2009.

(17) *Multi-Drug Resistance in Cancer*; Zhou, J., Ed.; Humana Press: New York, 2010.

(18) Lebedeva, I. V.; Pande, P.; Patton, W. F. *PLoS One* **2011**, *6*, No. e22429.

(19) Fardel, O.; Vee, M. L.; Jouan, E.; Denizot, C.; Parmentier, Y. *Expert Opin. Drug Metab. Toxicol.* **2015**, *11*, 1233−51.

(20) Richard, V.; Nair, M. G.; Santhosh, K. T. R.; Pillai, M. R. *BioMed Res. Int.* **2013**, *2013*, 517237.

DOI: 10.1021/acs.analchem.9b00388
Anal. Chem. 2019, 91, 4186−4194

(21) Yu, B.; Gu, D.; Zhang, X.; Li, J.; Liu, B.; Xie, J. *Oncotarget* **2017**, *8*, 27412−27427.
(22) Golebiewska, A.; Brons, N. H. C.; Bjerkvig, R.; Niclou, S. P. *Cell Stem Cell* **2011**, *8*, 136−47.
(23) Mo, S.-L.; Li, J.; Loh, Y. S.; Brown, R. D.; Smith, A. L.; Chen, Y.; Joshua, D.; Roufogalis, B. D.; Li, G. Q.; Fan, K.; Ng, M. C. H.; Sze, D.; Factors, M.-y. *Bone Marrow Res.* **2011**, *2011*, 524845.
(24) Sharom, F. J. *Biochem. Cell Biol.* **2006**, *84*, 979−92.
(25) Michelson, S.; Slate, D. *Bull. Math. Biol.* **1992**, *54*, 1023−38.
(26) Saengkhae, C.; Loetchutinat, C.; Garnier-Suillerot, A. *Biochem. Pharmacol.* **2003**, *65*, 969−77.
(27) Crompton, I. E.; Waley, S. G. *Biochem. J.* **1986**, *239*, 221−24.
(28) James, L. R.; Andrews, S.; Walker, S.; de Sousa, P. R.; Ray, A.; Russell, N. A.; Bellamy, T. C. *PLoS One* **2011**, *6*, No. e26889.
(29) Patela, T. P.; Mana, K.; Firestein, B. L.; Meaneya, D. F. *J. Neurosci. Methods* **2015**, *243*, 26−38.
(30) Neal, A. S.; Rountree, A. M.; Radtke, J. R.; Yin, J.; Schwartz, M. W.; Hampe, C. S.; Posner, J. D.; Cirulli, V.; Sweet, I. R. *Sci. Rep.* **2016**, *6*, 39319.
(31) Xu, G.; Zhong, Y.; Munir, S.; Yang, B. B.; Tsang, B. K.; Peng, C. *J. Clin. Endocrinol. Metab.* **2004**, *89*, 5523−34.
(32) Lacerda, L.; Pusztai, L.; Woodward, W. A. *Drug Resist. Updates* **2010**, *13*, 99−108.
(33) Rychlik, B.; Balcerczyk, A.; Klimczak, A.; Bartosz, G. *J. Membr. Biol.* **2003**, *193*, 79−90.
(34) Payen, L.; Delugin, L.; Courtois, A.; Trinquart, Y.; Guillouzo, A.; Fardel, O. *Br. J. Pharmacol.* **2001**, *132*, 778−84.
(35) Karunaratne, D. N.; Audus, K. L. *J. Natl. Sci. Found. Sri Lanka* **2007**, *35*, 19−27.
(36) Bartlett, J. W.; Frost, C. *Ultrasound Obstet. Gynecol.* **2008**, *31*, 446−75.
(37) Holder, D. J.; Marino, M. J. *Curr. Protoc. Pharmacol.* **2017**, *76*, A.3G.1.
(38) Nakano, A.; Tsuji, D.; Miki, H.; Cui, Q.; El Sayed, S. M.; Ikegame, A.; Oda, A.; Amou, H.; Nakamura, S.; Harada, T.; Fujii, S.; Kagawa, K.; Takeuchi, K.; Sakai, A.; Ozaki, S.; Okano, K.; Nakamura, T.; Itoh, K.; Matsumoto, T.; Abe, M. *PLoS One* **2011**, *6*, No. e27222.
(39) Teng, Y.; Hsieh, Y.; Hung, C.; Lin, H. *J. Agric. Food Chem.* **2015**, *63*, 847−55.
(40) Hanafi, R. S.; Lämmerhofer, M. *J. Chromat. A* **2018**, *1534*, 55−63.
(41) Luqmani, Y. A. *Med. Princ. Pract.* **2005**, *14* (suppl1), 35−48.
(42) Mansoori, B.; Mohammadi, A.; Davudian, S.; Shirjang, S.; Baradaran, B. *Adv. Pharm. Bull.* **2017**, *7*, 339−48.
(43) Koshkin, V.; Ailles, L. E.; Liu, G.; Krylov, S. N. *J. Cell. Biochem.* **2016**, *117*, 59−65.
(44) Koshkin, V.; Ailles, L. E.; Liu, G.; Krylov, S. N. *J. Cell. Biochem.* **2017**, *118*, 154−162.
(45) Hochberg, H.; Brody, Y.; Shav-Tal, Y. *Methods* **2017**, *120*, 58−64.
(46) Galievsky, V. A.; Stasheuski, A. S.; Krylov, S. N. *Anal. Chim. Acta* **2016**, *935*, 58−81.
(47) Galievsky, V. A.; Stasheuski, A. S.; Krylov, S. N. *Anal. Chem.* **2017**, *89*, 11122−11128.
(48) Niu, F.; Wang, D. C.; Lu, J.; Wu, W.; Wang, X. *J. Cell. Mol. Med.* **2016**, *20*, 1789−95.
(49) Wambre, E.; Bajzik, V.; DeLong, J. H.; O'Brien, K.; Nguyen, Q. A.; Speake, C.; Gersuk, V. H.; DeBerg, H. A.; Whalen, E.; Ni, C.; Farrington, M.; Jeong, D.; Robinson, D.; Linsley, P. S.; Vickery, B. P.; Kwok, W. W. *Sci. Transl. Med.* **2017**, *9*, No. eaam9171.
(50) Fadini, G. P.; Losordo, D.; Dimmeler, S. *Circ. Res.* **2012**, *110*, 624−37.
(51) Zou, B.; Sun, S.; Qi, X.; Ji, P. *Mol. Med. Rep.* **2012**, *5*, 1116−20.
(52) Haimeur, A.; Conseil, G.; Deeley, R. G.; Cole, S. P.C. *Curr. Drug Metab.* **2004**, *5*, 23−53.
(53) Doane, D. P.; Seward, L. E. *J. Stat. Edu.* **2011**, *19.2*, 1−18.

DOI: 10.1021/acs.analchem.9b00388
Anal. Chem. 2019, 91, 4186−4194

Supporting Information for:

Cytometry of Reaction Rate Constant (CRRC): Measuring Reaction Rate Constant in Individual Cells to Facilitate Robust and Accurate Analysis of Cell-Population Heterogeneity

Vasilij Koshkin, Sven Kochmann, Apinaya Sorupanathan, Chun Peng, Laurie E. Ailles, Geoffrey Liu, and Sergey N. Krylov

Table of Contents

Other Supporting Files

File name	Description/Experiment
Timeseries.zip	Images of time series experiments (TIF files)
Kinetictraces.zip	Kinetic traces extracted from time series images (CSV files)
Plotteddata.zip	Histogram data and plots (OPJ files)

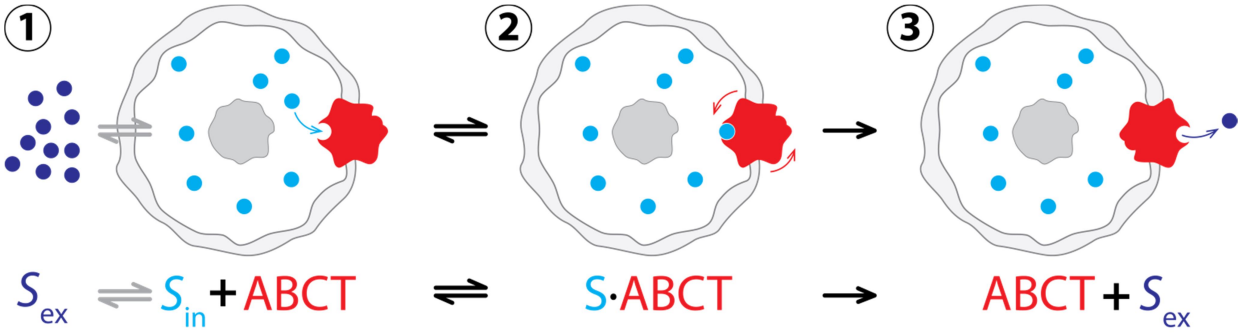

Figure S1. Schematic depiction of the MDR transport catalysed by ABC transporters (ABCT):
1) extracellular substrate (S_{ex}) and intracellular substrate (S_{in}) are in equilibrium with each other;
2) ABCT and S_{in} are forming a complex S•ABCT
3) S•ABCT is flipping and S_{ex} is released outside the cell.

Note S1: Extraction of kinetic traces from cell images

The time series, which are archived in timeseries.zip, were evaluated in five steps specified below. ImageJ software (1.46v; https://imagej.nih.gov/ij/) with the Time Series Analyzer V3 (https://imagej.nih.gov/ij/plugins/time-series.html) plugin was used for this evaluation.

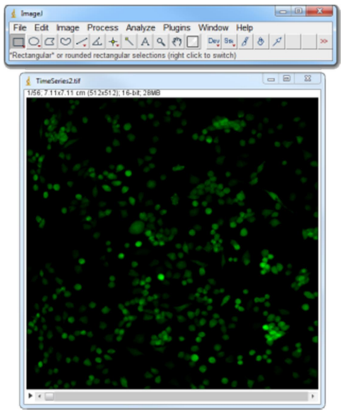

1. Opening the time-series in ImageJ.

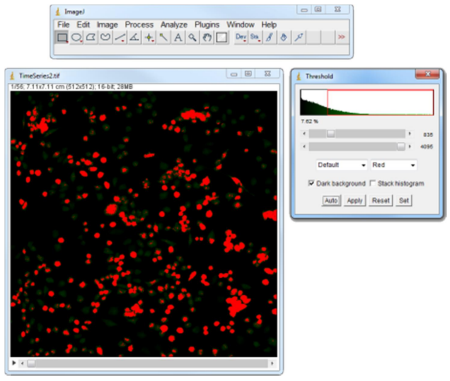

2. Adjusting the threshold (Image→Adjust→Threshold) to facilitate cell identification in the next step(s). We used "Auto" (*i.e.* IsoData algorithm) and adjusted the threshold to match manual cell count ("gold standard").

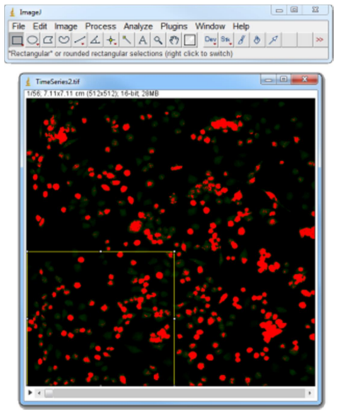

3. Due to technical limitations of the Time Series Analyzer plugin, only 149 cells could be analyzed at once. Therefore, we divided the time-series into sections (yellow rectangle in the example picture above) and analyzed them separately in ImageJ.

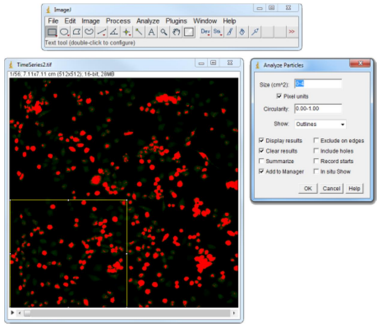

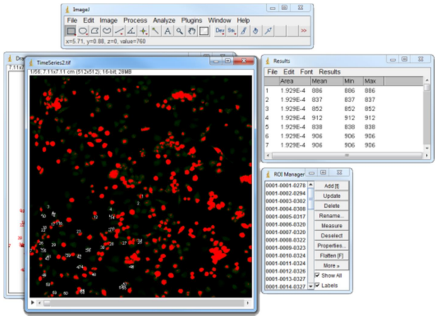

4. Analyzing particles (Analyze->Analyze Particles; do not process all images). Settings: Size: 0-4 (Pixel units); Circularity: 0.00-1.00; Show: Outlines; Display results; Clear results; Add to Manager.

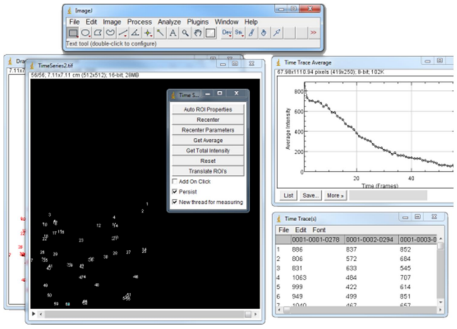

5. Running Time Series Analyzer plugin (we used Get Average) resulting in the time traces for each cell of the evaluated section (see Step 3) and a time trace average curve.

The sections of each time trace and the time traces of one experiment were merged into a single CSV file containing the kinetic curves of 1092 cells; CSV files of all traces can be found in kinetictraces.zip. We organized the traces in a manner similar to that of time series organization (see *Image acquisition* in the main text for more details).

Note S2: Analysis of kinetic traces

The kinetic traces were subjected to kinetic and non-kinetic assessment by OriginPro software (https://www.originlab.com). Among 1092 traces in each CSV file, there were a few that were not suitable for evaluation because of very fast fluorescence decay. They were excluded from further analysis, but each data set typically still contained over 1000 cells. This data were subjected to both kinetic and non-kinetic assessment.

The kinetic assessment is illustrated in Figure S2 below. The rate constant of leakage efflux (k_{leak}) was determined from a linear fit of the initial segment (red, I_0 to I_1). The cumulative rate constant (k_{total}) of the leakage process and MDR transport ($k_{leak} + k_{MDR}$) was determined from an exponential fit of the main segment (blue, I_1 to I_2) using *ExpDec1 function* constrained to non-negative y_0. The value of k_{MDR} was calculated by $k_{MDR} = k_{total} - k_{leak}$. For the majority of A2780 cells, the following relation was satisfied: $k_{leak} < 0.1 \times k_{total}$. It rendered the contribution of k_{leak} to k_{total} negligible in our system and the following was assumed $k_{total} \approx k_{MDR}$.

For the non-kinetic assessment, parameter $(I_1 - I_2) / I_1$ was determined for each kinetic trace.

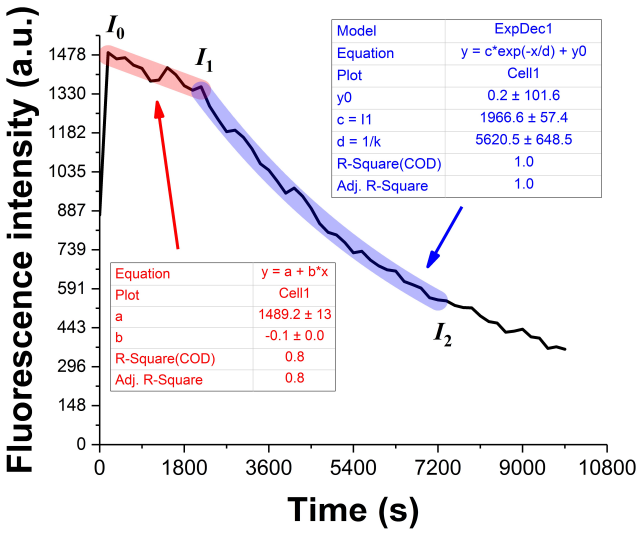

Figure S2. Example of finding k_{leak} and k_{MDR} from an experimental kinetic curve. The value of k_{leak} was found as $k_{leak} = -b / a$ (equals eq 3 in the main text). The value of k_{MDR} was found as $k_{MDR} = 1 / d$ (blue fitting function equals eq 5 in the main text).